A high throughput SEC23 functional interaction screen reveals a role for focal adhesion and extracellular matrix signalling in the regulation of COPII subunit SEC23A

Juan Jung[1], Muzamil Majid Khan[1,3], Jonathan Landry[2], Aliaksandr Halavatyi[2], Pedro Machado[2,4], Miriam Reiss[1,5], Rainer Pepperkok[1,2,3]

[1]Cell Biology Cell Biophysics Unit and [2]Core Facilities Unit, European Molecular Biology Laboratory, Meyerhofstraße 1, 69117 Heidelberg, Germany. [3] Lung Research Center Heidelberg (TLRC), German Center for Lung Research (DZL), Heidelberg, Germany. Current address: [4]Centre for Ultrastructural Imaging, King's College London, New Hunt's House, Guy's Campus, London SE1 1UL, UK. [5]University Clinics, Heidelberg University, Otto-Meyerhof-Zentrum, Im Neuenheimer Feld 350, 69120 Heidelberg, Germany

Address all correspondence to: juan.jung@embl.de or pepperko@embl.de

ABSTRACT

Proteins that enter the secretory pathway are transported from their place of synthesis in the Endoplasmic Reticulum (ER) to the Golgi apparatus by COPII coated carriers. The components of the COPII transport machinery have been well characterized, but the network of proteins that regulate these components have remained largely elusive. The discovery of such regulatory proteins is crucial for understanding how cells integrate intracellular and extracellular information to fine-tune membrane traffic in the secretory pathway. A key group of proteins that plays a central role in the regulation of membrane traffic is associated with the cytoskeleton. Using high throughput microscopy of the well-established VSVG transport from the ER to the plasma membrane, we comprehensively screened 378 cytoskeleton-associated proteins for their functional interaction with the COPII components SEC23A and SEC23B using a double knockdown approach. Ranking of the transport effectors identified 20 cytoskeleton-associated proteins as the strongest functional interactors of SEC23, most of them not previously associated with the secretory pathway. Six of the functional SEC23B interactors (FERMT2, NGEF, MACF1, MAPK8IP2, PIK3CA, ROCK1), which were previously functionally related to cell adhesion, strongly inhibited cargo export from the ER. Surprisingly, knockdown of these SEC23B interactors resulted in the downregulation of SEC23A, a SEC23 paralogue that has been implicated in the secretion of extracellular matrix components. Furthermore, SEC23A downregulation could also be achieved by plating cells on extracellular matrix (ECM) and was dependent on focal adhesions function. Altogether, our results identify a network of cytoskeleton-associated proteins connecting ECM related signalling with the gene expression of the COPII secretory machinery.

INTRODUCTION

The secretory pathway is responsible for the delivery of lipids and proteins to their correct location, including the plasma membrane, extracellular space and many membrane-bounded organelles. This allows the cells to dynamically regulate the size, composition and function of those compartments. Alterations in the secretory pathway play important roles in a number of diseases including cancer, fibrosis and neurodegenerative

disorders (for reviews see (De Matteis and Luini 2011; Yarwood et al. 2020), and understanding how cells integrate different internal and external stimuli to fine-tune secretion remains a central question in cell biology and disease mechanisms.

In the early secretory pathway, proteins are transported from their place of synthesis in the ER to the Golgi apparatus in a process mediated by COPII coated carriers. COPII assembly is initiated by the binding of the GTPase SAR1 to specific sites of the ER termed ER exit sites (ERES), followed by the recruitment of an inner coat composed of SEC23-SEC24 dimer responsible for cargo sorting and an outer coat composed of SEC13-SEC31 that provides a structural scaffold for membrane deformation and carrier formation (see (Miller and Schekman 2013) and references therein).

At ERES, protein secretion is regulated through an expanded COPII protein interaction network that ensures secretion meets physiological demands. For instance, nutrient deprivation reduces secretion by decreasing the number of ERES (Zacharogianni et al. 2011). Conversely, growth factor signalling increases the number of ERES and prepares the cells for a higher secretory demand (Farhan et al. 2010; Tillmann et al. 2015). More recently, Epidermal growth factor receptor (EGFR) signalling has also been linked to the transcriptional regulation of the COPII machinery in response to extended EGFR degradation to restore efficiently the availability of EGFR at the plasma membrane (Scharaw et al. 2016).

The cytoskeleton plays important roles in the organization and function of the secretory pathway by acting as a scaffold for membrane deformation, carrier transport and organelle positioning (Anitei and Hoflack 2012; Gurel, Hatch, and Higgs 2014; Fourriere et al. 2020). For example, it has been shown that SEC23 interacts with DCTN1 (p150-glued), a subunit of the dynactin complex which links the COPII machinery to the microtubules, facilitating the long-distance movement of carriers towards the Golgi (Watson et al. 2005). A role of this SEC23-DCTN1 interaction in cargo concentration at ERES independent of microtubules has also been proposed (Verissimo et al. 2015). Moreover, a key role of the cytoskeleton and associated proteins that has been less explored in the context of the regulation of the secretory pathway is the integration of extracellular and intracellular information (Moujaber and Stochaj 2019) including, for instance, mechanotransduction (Sun, Guo, and Fässler 2016), metabolism and signalling (Janmey 1998). In order to systematically and comprehensively explore the functional interactions of the cytoskeleton and associated factors with the transport machinery of the early secretory pathway, we conducted a functional siRNA-based interaction screen exploring possible synergistic functional interactions of 378 cytoskeleton and associated proteins with the COPII components SEC23A or SEC23B. Our results reveal an unexpected transcriptional regulation of the COPII subunit SEC23A by cytoskeleton-related proteins involved in focal adhesions and ECM function.

RESULTS

Identification of cytoskeleton-related proteins functionally interacting with SEC23A/B

Single siRNAs targeting altogether 378 cytoskeleton and associated proteins were co-transfected with siRNAs targeting *SEC23A* or *SEC23B* and biosynthetic transport of the vesicular stomatitis virus G protein (VSVG) from the ER to the cell surface (Kreis and Lodish 1986) was quantified as previously described (Simpson et al., 2012) (**Fig. 1A**). In order to identify synergistic functional interactors of SEC23A or SEC23B, the siRNA concentrations and transfection conditions were chosen such that siRNA transfection of *SEC23A* or *SEC23B* targeting siRNAs alone did not significantly affect VSVG transport compared to control transfected cells (**Fig. 1B**). However, co-transfection of siRNAs targeting *SEC23A* and *SEC23B* under these conditions caused significant transport inhibition of VSVG at the ER level (**Fig. 1B** and **Fig. 2**) consistent with their role in cargo

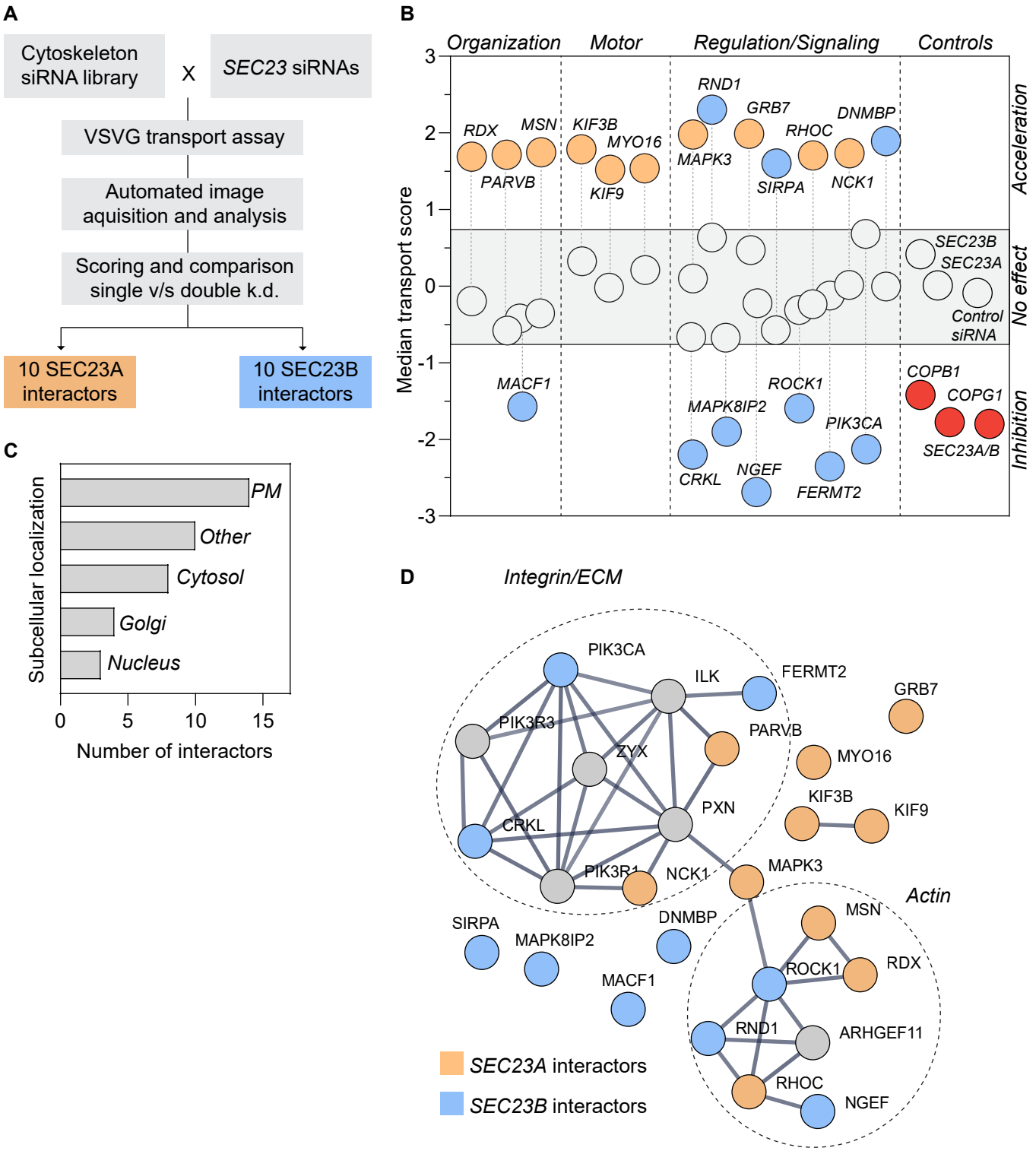

Figure 1. A functional interaction screen between SEC23 and cytoskeleton-associated proteins
(A) HeLa cells were co-transfected with siRNAs targeting 378 cytoskeleton-associated proteins and siRNAs targeting the COPII subunits SEC23A or B. Using and automated microscopy acquisition and analysis pipeline, VSVG transport to the cell surface was quantified after 60 hrs of depletion in single and double knockdowns conditions. For each condition, a transport score was calculated. **(B)** The conditions in which the double knockdown score was significantly different from the expected additive effect of the single knockdowns were selected. Grey circles denote single knockdowns. Red circles denote the positive controls. Interactors in double knockdown are shown in orange (SEC23A interactors) or blue (SE23B interactors). **(C)** Annotation of the subcellular location of the interactors using the Human Protein Atlas and Compartments as the main sources. For proteins with multiple locations, only the two main locations were annotated (PM=Plasma membrane). Others include mitochondria, centrioles, focal adhesions, etc. **(D)** STRING network (Szklarczyk et al. 2019) using medium confidence and removing the text mining. Proteins in grey are not interactors but were included to fill up the gaps in the network.

sorting and concentration at ERES.

Analysis of more than 85.000 images allowed a ranking of the genes targeted by the respective siRNAs according to their effect on VSVG transport when co-knocked down with either *SEC23A* or *SEC23B* (**Table 3**). Comparing transport rates of double knockdowns to single knockdowns and ranking of the strongest transport effectors revealed 20 cytoskeleton related genes in which VSVG transport in the double knockdown (SEC23A or SEC23B + cytoskeleton (associated) protein) was significantly different from the additive effect one would expect from the results of the single knockdowns (**Fig. 1B**) (See material and methods for more details of the screen and data analysis).

The synergistic behaviour in transport induced by the siRNA depletion strongly suggests a functional interaction between SEC23 and the 20 cytoskeleton related proteins selected by ranking, henceforth we call these proteins SEC23 functional interactors. We found SEC23 functional interactors that, in the double knockdown, led to transport acceleration, while others led to transport inhibition. Interestingly, VSVG transport inhibitors were only identified as functional interactors with SEC23B and no overlap between SEC23A and SE23B interactors was observed (**Fig. 1B and Table 3**). The results of the screen are available in the **Table 2.**

Annotation of the subcellular location using existing information in Compartments (Binder et al. 2014) and the Human Protein Atlas (Thul et al. 2017) shows that many of the interactors are proteins located at the plasma membrane with a few also localizing to the Cytosol, Nucleus or Golgi complex (**Fig. 1C**). Interestingly, none of the SEC23 functional interactors were annotated to localize to the ER or ER-exit sites as their main locations, which is the place of function for the COPII complex. While some of the interactors are motor proteins (KIF9, MYO16, KIF3B) or proteins that participate in the organization of the cytoskeleton (MACF1), most of the interactors are proteins involved in signalling pathways (**Fig. 1B**) that regulate the cytoskeleton in response to diverse stimuli including growth factor, actin signalling and cell-matrix interactions (**Fig. 1D**). With the exception of PIK3CA, ROCK1 and MACF1 these proteins have not been functionally implicated previously in the secretory pathway. Also, and in agreement with our previous genome wide screen (Simpson et al. 2012), depletion of these proteins alone does not affect VSVG transport (**Fig. 1B**).

Functional SEC23B interactions occur at the ER exit level

For proteins causing an inhibition of VSVG transport in the double knockdown experiments, the intracellular location of VSVG was assessed, as the place of VSVG inhibition in the secretory pathway is expected to give first insights into the mechanisms of how the respective target genes may functionally interact with SEC23B. For 6 out of the 7 SEC23B functional interactors tested (FERMT2, MACF1 MAPK8IP2, NGEF, PIK3CA and ROCK1) VSVG was largely retained in the ER, similar to double knockdown of SEC23A and SEC23B, while in control transfected cells VSVG was observed mainly at the plasma membrane (**Fig. 2**). Only for the double knockdown of SEC23B and CRKL, post-ER structures could be observed (**Fig. 2**). The striking similarity of the phenotypes for almost all of these functional SEC23B interactors suggests that there might be a common mechanism or pathway by which these functionally diverse proteins interact with SEC23B.

To gain more insight into the functional interactions we focused our analyses next on MACF1, as this protein has been previously also functionally implicated in the secretory pathway. MACF1 is a microtubule-actin cross-linker (Leung et al. 1999; Karakesisoglou, Yang, and Fuchs 2000) localized at focal adhesions and cell periphery but also present at the Golgi complex (Lin et al. 2005) where it has been proposed to be involved in Golgi complex to plasma membrane transport (Kakinuma et al. 2004; Burgo et al. 2012). To characterize the MACF1/SEC23B transport impairment in more detail, the VSVG transport marker was released from the ER for 5 and 10 minutes only. In control cells, transfected with non-targeting siRNA, VSVG appeared in post-ER

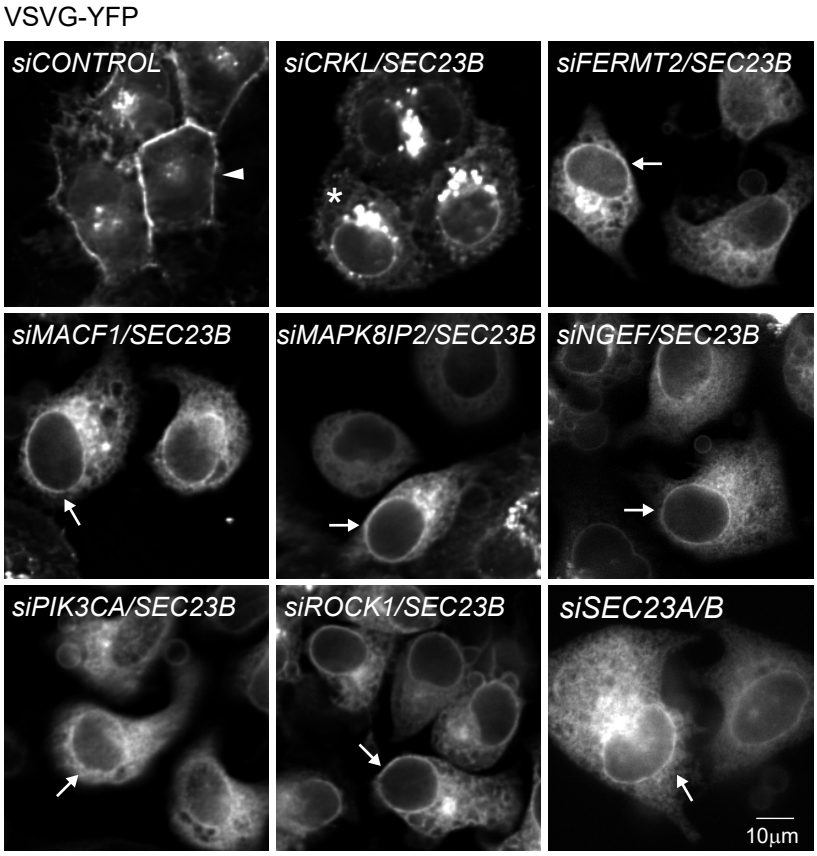

Figure 2. VSVG localization for the SEC23B interactors that promote transport block
Widefield images of VSVG-YFP after 1 hr of temperature shift from 40ºC to 32ºC. Transport was assessed after 60 hrs of knockdown with the indicated siRNAs. Arrow indicate ER membranes. Arrowheads indicate plasma membrane. Asterisk indicates Golgi or Post-Golgi membranes.

punctate structures visible already at 5 minutes after temperature shift, and a substantial amount of VSVG accumulated in the perinuclear region at 10 minutes, most likely representing the Golgi complex. In the case of MACF1/SEC23B double knockdown cells, occasional post-ER punctate structures became only visible at 10 min after the temperature shift and accumulation of the marker in the Golgi complex area apparently did not occur (**Fig. 3A**). Consistent with this transport impairment at the ER level upon MACF1/SEC23B double knockdown, we observed a reduction in the number of SEC31 positive ERES and reduction of COPI positive ER to Golgi complex transport intermediates compared to control transfected cells or cells transfected with the respective siRNAs alone (**Fig. 3B, C)**. Moreover, P24, a cargo receptor that recycles between the Golgi complex and the ER, shifts its distribution to a more ER-predominant localization (**Fig. S1A)**. In MACF1/SEC23B double knockdown cells the Golgi marker GM130 appeared more dispersed compared to control transfected cells (**Fig. S1B**). No apparent changes were observed for the endosomal marker EEA1 (**Fig. S1C**). To confirm the transport inhibition observed for VSVG independently, we quantified the transport of E-Cadherin to the plasma membrane using the established inducible transport system RUSH (Boncompain et al. 2012). MACF1/SEC23B double knockdown showed a reduction of E-Cadherin transport between 40-70 %, depending on the siRNA used, while the single knockdowns did not show a significant transport alteration (**Fig. 4A**). In agreement with the data obtained for the transport marker VSVG, the majority of E-Cadherin was retained in the ER at time-points when in control transfected cells the transport marker already accumulated in post-ER structures resembling most likely the Golgi complex (**Fig. 4B**). Moreover, in the absence of any overexpressed cargo, electron microscopy analyses show that in MACF1/SEC23B double knockdown cells, the ER becomes often bloated, characteristic of a transport block at the ER level (see e.g. Fujiwara et al. 1988; Zhang et al. 1994) (**Fig. 4C**).

Next, we asked whether MACF1 and SEC23B functional interaction is due a physical interaction. While most of the MACF1 staining is located in the cytosol, cell periphery and Golgi (as previously described) with no significant staining in the ER or peripheral exit sites, we cannot discard colocalization with exit sites in the densely populated perinuclear region (**Fig. S2A**). To test if MACF1 and SEC23B interact physically we performed Co-IP experiments but we failed to detect an interaction under our experimental conditions (**Fig. S2B**). While these results do not exclude completely the possibility of physical interaction of SEC23B and MACF1 they suggest that the functional interaction of these two proteins as observed here is most likely indirect.

Knockdown of SEC23B functional interactors downregulates SEC23A

The striking similarity of the phenotypes for almost all of the SEC23B functional interactors causing a VSVG transport inhibition in the double KD experiments suggests that there might be a common mechanism or pathway by which these proteins functionally interact with SEC23B. Based on their localization and functional annotation reported in the literature, we considered them unlikely to be direct interactors of SEC23B, although this possibility cannot be rigorously excluded. We speculated that their knockdown in cells may affect factors that are more directly related to the membrane traffic machinery in the early secretory pathway. As a first step to investigate this hypothesis, we performed mRNA sequencing to explore the transcriptional changes induced by depletion of the SEC23B functional interactors alone and testing if knockdown of the various SEC23B functional interactors might cause overlapping transcriptional changes. With a p-adjusted value of 0.1 and a Log2 fold change above 0.58 or below -0.58, we found significant changes in gene expression for all the knockdowns tested (**Fig. S3A** and **Table 4** for the gene list). As expected, depletion of a protein with pleiotropic functions like PIK3CA generated the biggest changes (i.e. 419 genes downregulated and

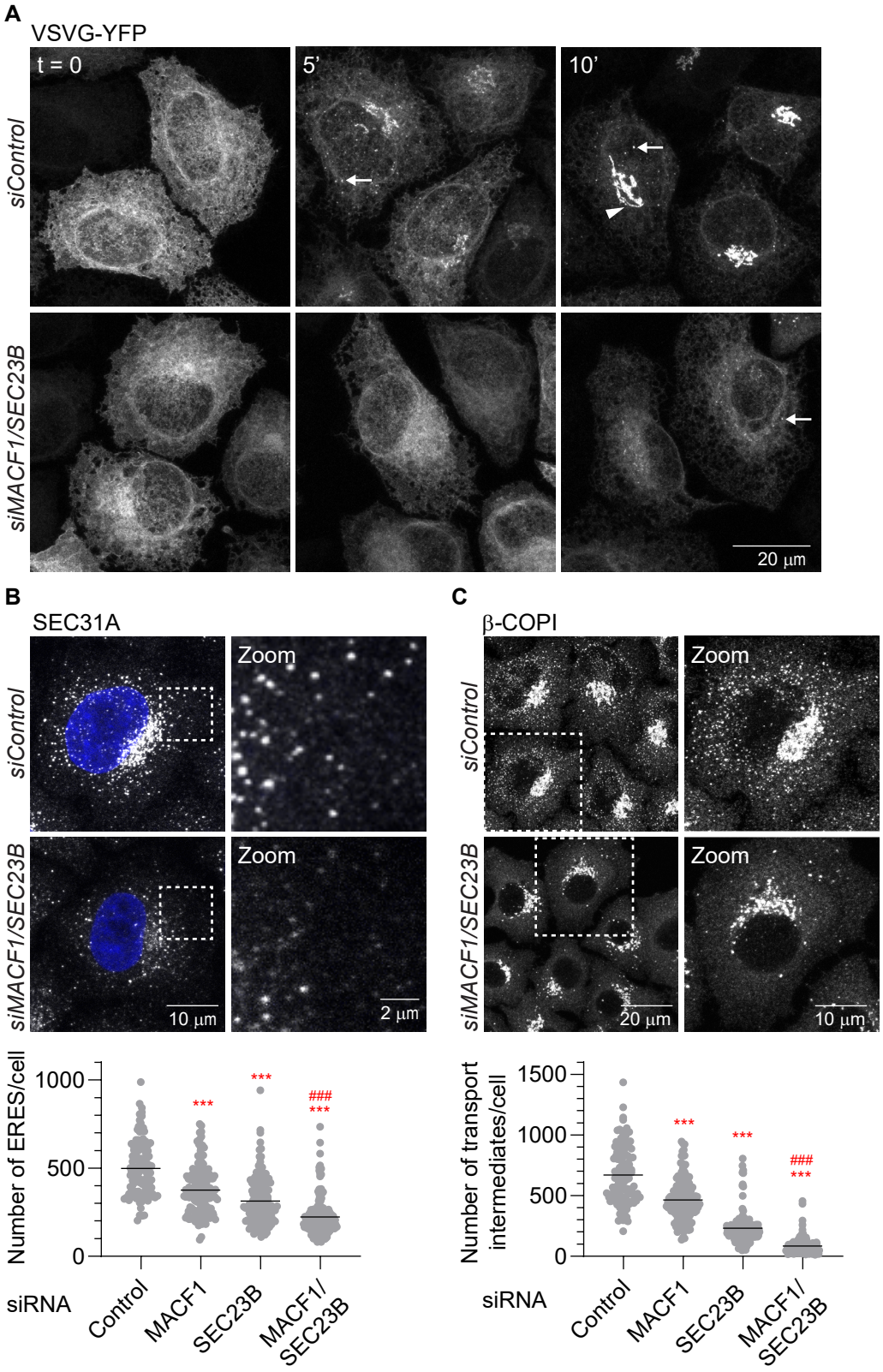

Figure 3. MACF1 and SEC23B co-depletion causes an ER exit block

(A) Confocal images of VSVG-YFP after 5 and 10 min of temperature shift from 40ºC to 32ºC. Transport was assessed after 60 hrs of knockdown with the indicated siRNAs. Arrows indicate puncta most likely representing transport intermediates. Arrowheads indicate juxtanuclear structures most likely representing Golgi. (B) Confocal images and quantification of ERES assessed by SEC31A staining after 48 hrs of knockdown with the indicated siRNAs. (C) Confocal images and quantification of transport intermediated assesed by beta-COPI staining after 48 hrs of knockdown with the indicated siRNAs. Statistical significance: *** p<0.001 compared to control. ### p<0.001 compared to SEC23B or MACF1 single knockdowns, Student´s t-test.

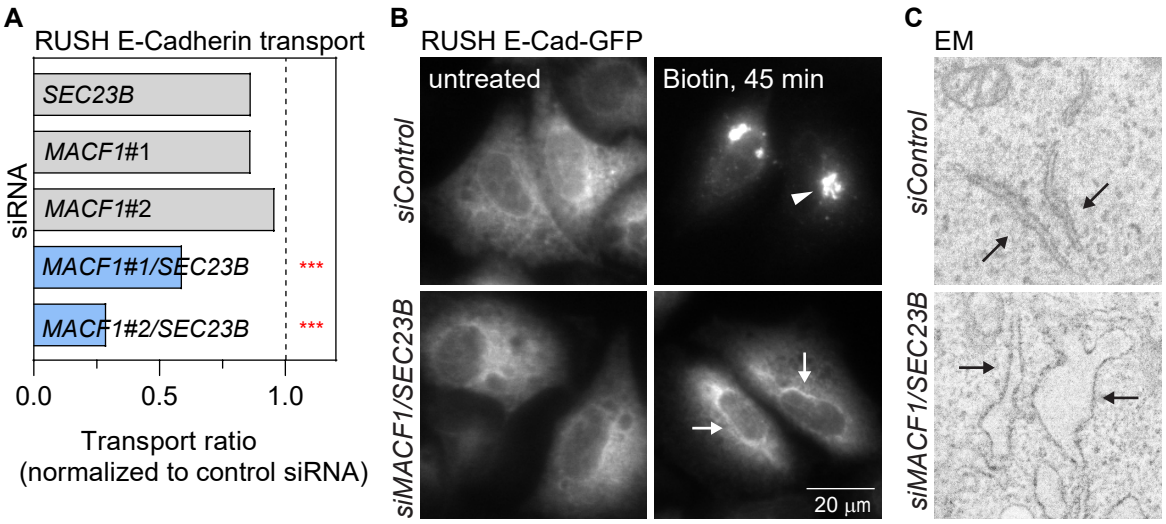

Figure 4. MACF1/SEC23B transport block is cargo independent

(A) E-Cadherin-GFP RUSH assay was performed after 48 hrs of knockdown with the indicated siRNAs. E-Cadherin-GFP transport was measured after 45 min of biotin release. The bars represent the transport average of one representative experiment in which > 500 cells per condition were quantified and normalized to control siRNA. Statistical significance: *** $p<0.001$ Student´s t-test. **(B)** Widefield images from the RUSH assay. Arrows indicate ER membranes. Arrowheads indicate post-ER structures. **(C)** Electron microscopy images of cells treated with the indicated siRNAs for 48 hrs. Arrows indicate ER membranes. The bloated ER in the MACF1/SEC23B double knockdown is characteristic of ER transport block.

580 genes upregulated). Also, out of the approx. 2300 genes differentially expressed across all 7 conditions tested, we observed little overlap between the transcriptional profiles (**Fig. S3B**).

To find a possible cause for the observed transport block when any of these SEC23B functional interactors were doubled knocked-down with SEC23B, we started by focusing our analysis of the transcriptome data on a set of 595 secretory pathway-related genes based on a recently annotated gene list (Feizi et al. 2017). Overall, the transcriptional changes observed for those genes were relatively minor with no particular enrichment of these genes or parts of them in any condition (Fisher's exact test). Surprisingly, we found that *SEC23A* was significantly downregulated in 6 of the 7 SEC23B functional interactors causing VSVG transport inhibition (**Fig. 5A** and **Table 5**). Most remarkably, *SEC23A* was found to be the only common gene that was affected by knockdowns of all the 6 SEC23B interactors tested. The downregulation of *SEC23A* upon knockdown of the SEC23B functional interactors could also be confirmed independently by RT-qPCR (**Fig. 5B**). Also, human lung fibroblasts treated with *MACF1* siRNA for 48 hours show reduced levels of *SEC23A* compared to control-treated cells (**Fig. 5B).** The downregulation in *SEC23A* mRNA levels induced by depletion of the functional SEC23B interactors was also accompanied by a downregulation of SEC23A at the protein level **(Fig. 5C)** which offers a straightforward explanation for the ER block in the double knockdown experiments described here, namely, reduction in the levels of total SEC23 by direct downregulation of *SEC23B* and an indirect downregulation of *SEC23A* (**Fig. 5D**). However, we cannot exclude the possibility that changes in other genes than *SEC23A* also contribute to the transport inhibition phenotype observed here.

ECM related cues lead to SEC23A downregulation

The decrease in SEC23A induced by the depletion of cytoskeleton regulatory and associated proteins, suggests that cytoskeleton-related cues are connected to SEC23A gene expression. But which are these cues? Using Metascape (Zhou et al. 2019) we performed enrichment analysis on the mRNA-Seq data to look for the most relevant processes affected as a consequence of the depletion of the SEC23B functional interactors. We found that the most common process enriched among the analyzed SEC23B functional interactors were cell adhesion, negative regulation of cell proliferation and blood vessel development (**Fig. 6A** and **Table 6** for the full list**)**. We decided to focus on cell adhesion as it is a process that is directly connected to the cytoskeleton and some of the SEC23B functional interactors have a well-established link to it. For instance, MACF1 has been associated with focal adhesions dynamics (Wu, Kodama, and Fuchs 2008) and FERMT2 regulates integrin-dependent cell-matrix attachment (Tu et al. 2003; Montanez et al. 2008). In fact, 4 out of 6 of the SEC23B functional interactors are bona fide members of the adhesome (Zaidel-Bar et al. 2007), which currently includes 232 proteins known to be an integral part of focal adhesions (FAs) or associated to them (www.adhesome.org) (**Fig. 6B**). Consistent with this, in the MACF1 knockdown cells, enlarged focal adhesions were observed, in agreement with a knock out mouse model described earlier (Wu, Kodama, and Fuchs 2008). Similarly, knockdown of all the other SEC23B functional inhibitors causing ER transport inhibition similar alterations of FAs were observed (**Fig. 7A**). As changes in FAs are dependent on interactions with ECM as shown in **Fig. 7B and C** (see also review by (Geiger, Spatz, and Bershadsky 2009)) we hypothesized that SEC23A might be sensitive to this interaction. To test this more directly we plated cells specifically on different ECMs and measured the levels of *SEC23A* by RT-qPCR. Cells plated on Matrigel or in fibroblast derived-ECM showed reduced *SEC23A* mRNA levels compared to cells plated on plastic alone (**Fig. 7D**). Interestingly the Matrigel-mediated downregulation of *SEC23A* could be prevented by treatment with the focal adhesion kinase (FAK) inhibitor PND-1186 (**Fig. 7D**). Collectively, these results suggest that cell attachment to ECM regulates the levels of SEC23A in a process that involves FA signalling.

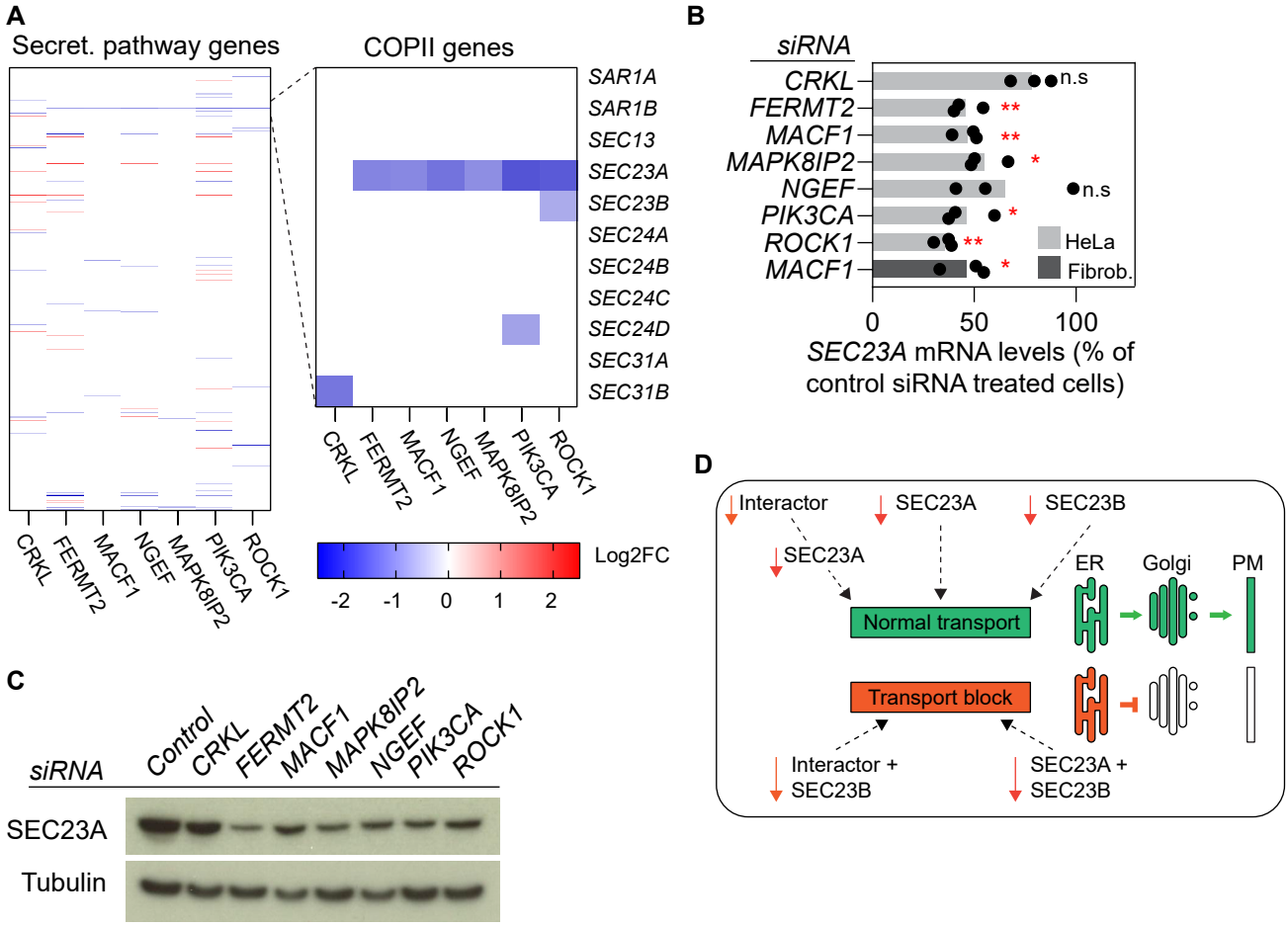

Figure 5. Depletion of functional interactors leads to SEC23A downregulation

(A) Differential expression analysis of a subset of 595 manually curated secretory pathway genes for the indicated knockdowns (48 hrs) compared to control siRNA. The zoomed-in region highlights the COPII genes. **(B)** RT-qPCR quantification of SEC23A levels after 48 hrs of knockdown with the indicated siRNAs. Bars represent averages of 3 independent experiments and the dots the individual values. The dark grey bar represents SEC23A levels after 48 hrs of MACF1 siRNA treatment in human lung fibroblasts. **(C)** Western-Blot analysis of SEC23A protein levels after 48 hrs of depletion with the indicated siRNAs. Alpha tubulin was used as a loading control. **(D)** Cartoon representing the transport phenotypes obtained during the screen and their relationship to SEC23A and SEC23B levels. Statistical significance: * $p<0.05$, ** $p<0.01$ compared to control, Student´s t-test.

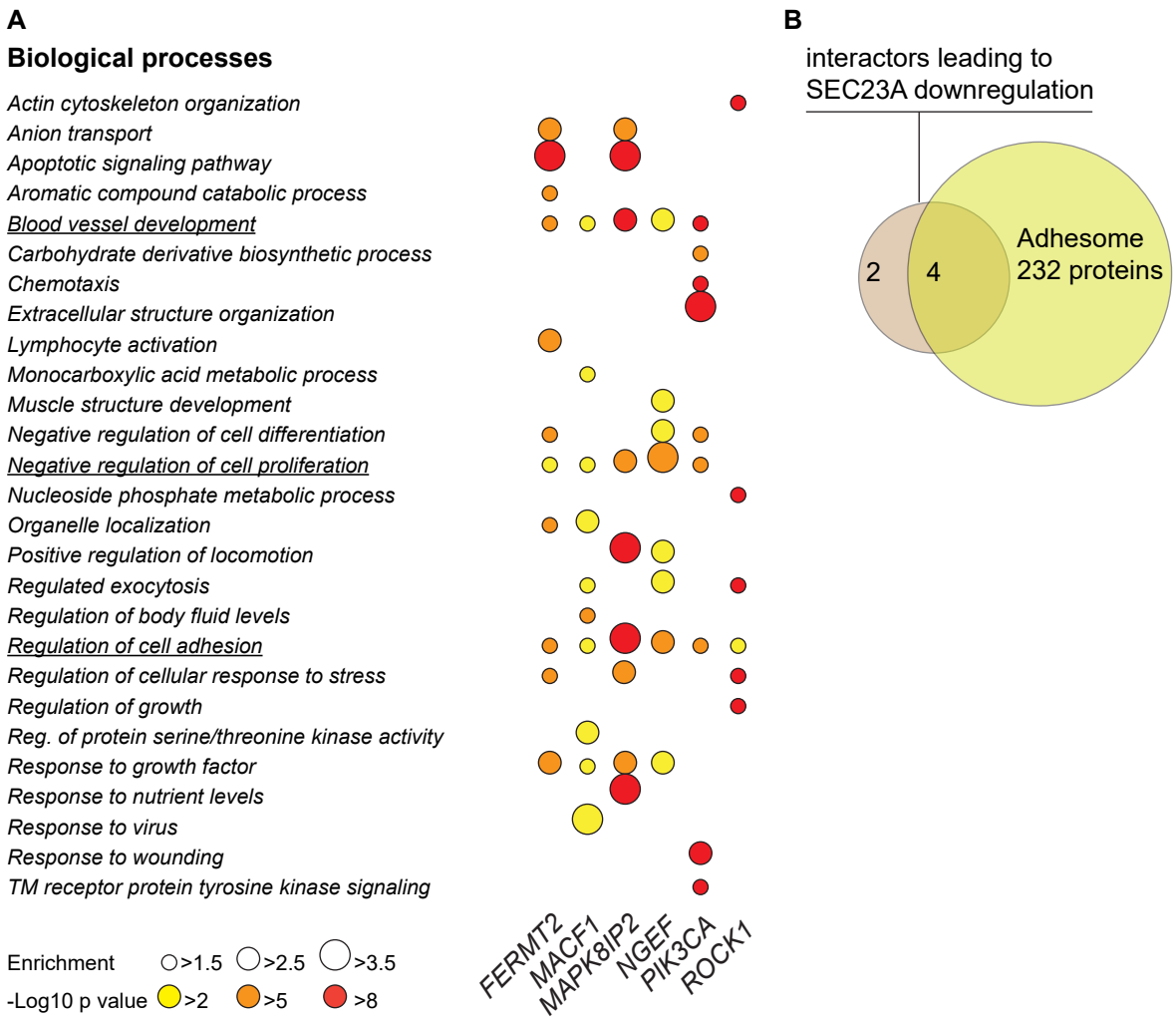

Figure 6. Enrichment analysis for the mRNA-Seq data

(A) The gene enrichment analysis was done using Metascape. GO terms for biological processes with a minimum enrichment of 1.5 and a minimum p-value of 0.01 are depicted. When possible, child terms were used over parents and redundant pathways were omitted. The most common processes across all 6 conditions are underlined **(B)** Venn diagram representing the intersection between the 6 interactors and the adhesome proteins

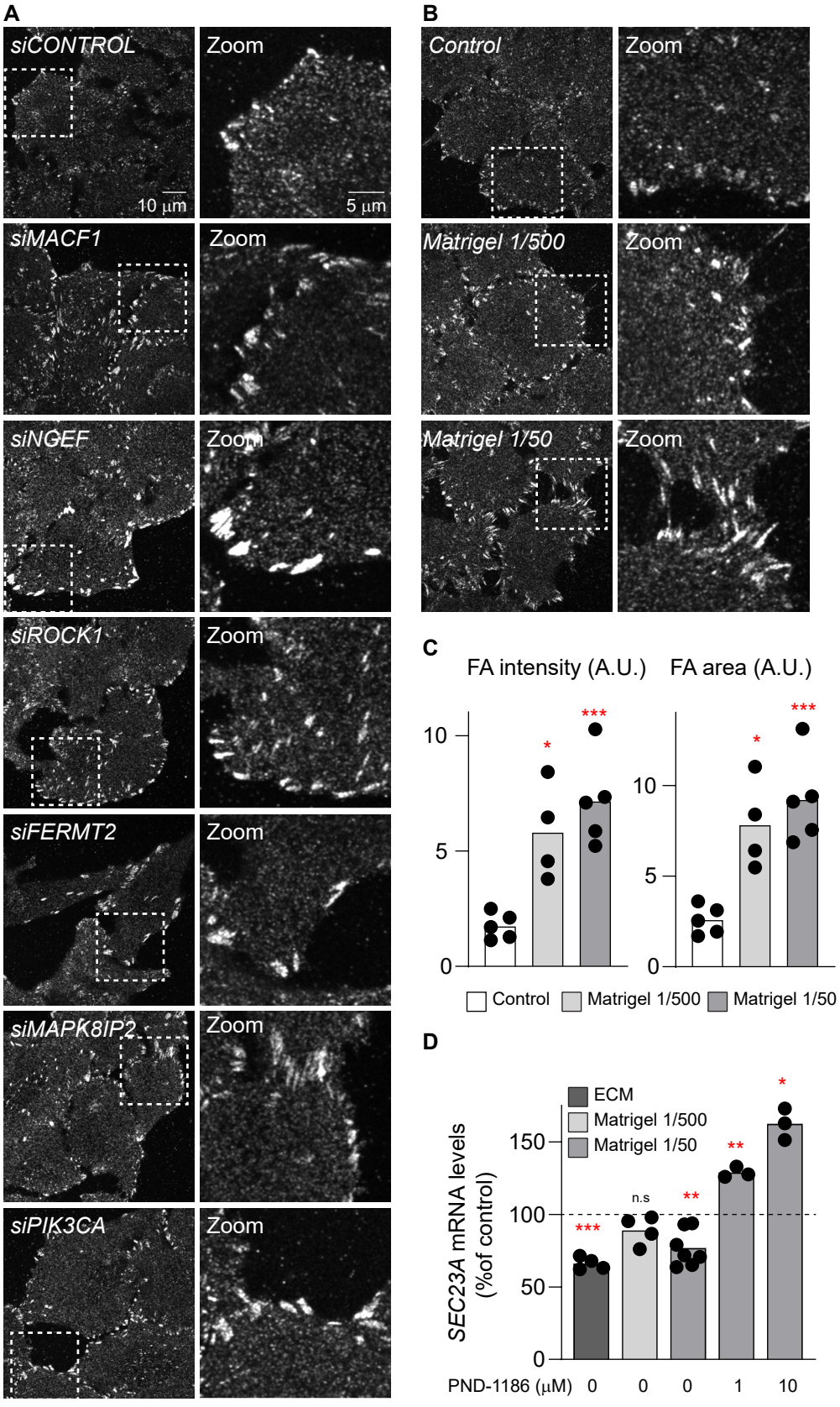

Figure 7. Cell attachment to ECM leads to SEC23A downregulation

Confocal images of focal adhesions assed by vinculin staining after 48 hrs of treatment with the indicated siRNAs **(A)** or after 24 hours of attachment to Matrigel-coated plates **(B)**. **(C)** Quantification of the focal adhesions shown in B. **(D)** SEC23A mRNA levels assessed by RTqPCR after 48 hours of seeding cells in dishes coated with Matrigel or Fibroblast derived ECM and treated with the FAK inhibitor PD-1186 for 24 hrs at the indicated concentrations. Statistical significance: * p<0.05, ** p<0.01 and ***p<0.001 compared to control, Student´s t-test.

DISCUSSION

In this work, we have studied the functional interaction of cytoskeleton-related proteins with the COPII subunits SEC23A or SEC23B in the early secretory pathway. This uncovered, amongst others, six strong SEC23B functional interactors that have been proposed to be functionally involved in cell attachment to ECM through focal adhesions. Surprisingly, single knockdowns of each of these proteins did not only lead to a change in expression of a number of genes, as expected when ECM regulators are perturbed but also to the transcriptional down-regulation of *SEC23A*. While these results provide a plausible explanation of our screening results showing that co-downregulation of any of these proteins with SEC23B causes a strong transport inhibition at the ER level, most likely due to a strong depletion of both SEC23 paralogues, these results also contribute to our understanding how cells integrate extracellular information such as ECM signalling into the secretory pathway an expands the increasing set of cues that are proposed to regulate the early secretory pathway including nutrient sensing (Zacharogianni et al. 2011; Liu et al. 2019) and growth factor signalling (Farhan et al. 2010; Tillmann et al. 2015; Scharaw et al. 2016).

Previous work clearly demonstrated a significant role of microtubules and associated microtubule motor proteins as facilitators of biosynthetic membrane traffic in the early secretory pathway (Scales, Pepperkok, and Kreis 1997; Presley et al. 1997; Watson et al. 2005; Verissimo et al. 2015). Therefore, we expected to find in our screen here a number of proteins with a more canonical role in the cytoskeleton, such as motor or alike proteins. However, the proteins we identified as the strongest functional interactors of the SEC23 homologues in ER to plasma membrane transport are described as regulators of signalling pathways at the plasma membrane. Motor and alike proteins were also identified as SEC23 functional interactors in our screen, however, with a much weaker effect on VSVG transport than those proteins we ranked as the strongest 20 SEC23 functional interactors.

Double knockdown siRNA-based functional interaction approaches have been used by others to identify complex networks underlying, for instance, cholesterol metabolism (Zimon et al., 2020, https://doi.org/10.1101/2020.10.29.360818), cancer (Laufer et al. 2013) or chromatin remodelling (Roguev et al. 2013). This strategy led us here to the identification of 20 cytoskeleton related proteins that functionally interact strongly with either SEC23A or SEC23B in the transport of the well-characterized cargo model VSVG. The majority of these 20 proteins have not been previously functionally implicated in the secretory pathway. Furthermore, none of them were identified as hits in an earlier genome-wide siRNA screen which identified altogether several hundred human genes directly or indirectly involved in biosynthetic transport from the ER to the plasma membrane (Simpson et al. 2012) or in another genome wide screen in Drosophila (Bard et al. 2006). Altogether, this demonstrates the potential of such double knockdown functional interaction screens as a tool to identify new regulators of the processes under view.

In order to better understand how each of the 6 cytoskeleton-associated proteins (FERMT2, MACF1, MAPK8IP2, NGEF, PIK3CA and ROCK1), which functionally strongly interact with SEC23B, could cause transport inhibition when co-downregulated with SEC23B, we analysed the transcriptional changes of cells upon single knockdown of these genes. Despite the fact that gene knockdown resulted in expression changes of hundreds of genes in each case, genes downregulated in common were rare with the exception of SEC23A, which was downregulated by each of the single knockdowns. This provides a plausible explanation for the synergistic effect of these knockdowns with SEC23B depletion, as cells lacking both SEC23 paralogues are not able to assemble COPII coats and cannot transport cargo out of the ER. Therefore, we propose these 6 proteins functionally interact with SEC23B because they are involved in the regulation of SEC23A levels.

This raises the question of how these apparently diverse proteins are functionally linked to the expression of SEC23A. Our transcriptome analyses of knockdown cells suggested that cell adhesion is a common process connected to the depletion of these 6 proteins. This hypothesis is also supported in the literature. For instance, FERMT2 is located at FAs and participates in the connection of ECM to the actin cytoskeleton through integrins (Tu et al. 2003), MACF1 crosslinks actin and microtubules at FAs (Wu, Kodama, and Fuchs 2008), ROCK1 is involved in stress fibre and FAs formation (Amano et al. 1997) and PIK3CA is a bona fide member of the FA interactome (www.adhesome.org). Independent experiments here, in support of the hypothesis that ECM signalling leads to modulation of SEC23A expression, showed that plating cells on fibroblast-derived ECM or Matrigel led to the downregulation of *SEC23A* and treatment of cells with a FAK inhibitor prevented the Matrigel-induced downregulation of *SEC23A*.

The role of FAs in the interpretation of ECM-related cues is well established (Geiger, Spatz, and Bershadsky 2009). FAs have also been involved in membrane trafficking including endocytosis and exocytosis (Wickström and Fässler 2011; Nolte, Hoen, and Margadant 2020). In exocytosis, FAs appear to serve as hot spots for secretion, a function that might be linked to the role of FAs in the organization of microtubules from TGN to the PM (Stehbens et al. 2014; Fourriere et al. 2020; Eisler et al. 2018). Based on our results here, we propose that ECM and FAs are also connected to membrane trafficking through the regulation of SEC23A expression. These views are complementary and contribute to understand how cells can link trafficking and extracellular cues in a robust manner. The precise molecular mechanisms that connect ECM to the expression of SEC23A remain to be investigated.

Interestingly, our results here show an apparent lack of overlap between SEC23A and SEC23B functional interactors. Although these two SEC23 paralogues are 85% identical at the amino acid sequence level, they have been proposed to have different functions in terms of cargo specificity. SEC23A has been proposed to mediate transport of extracellular matrix components, specifically collagens (Boyadjiev et al. 2006; Lang et al. 2006) and SEC23B has been shown to be specifically involved in the maintenance of professional secretory tissues like the pancreas (Khoriaty et al. 2016, 2017) or to the transport of EGFR (Scharaw et al. 2016). However, this view has been recently challenged by demonstrating an indistinguishable protein interactome of the two paralogues and the possibility to exchange the protein domains amongst them without functional losses (Khoriaty et al. 2018). It was proposed instead that the SEC23 paralogues may underlie different transcriptional regulation which could in part explain the distinct phenotypes of SEC23A/B deficiency within and across species different (Khoriaty et al. 2018). Our results here support these findings as, first, the knockdown of SEC23A or SEC23B alone did not result in a significant transport inhibition of VSVG, suggesting that the remaining paralogue is able to replace at least partially the function of its counterpart under the conditions used here. Only the depletion of SEC23A by the knockdown of the SEC23B functional interactors and in parallel knockdown of SEC23B resulted in a strong inhibition of transport. Second, linking the ECM with the expression of SEC23A at the transcriptional level, as suggested by our results here, offers a potentially interesting feedback mechanism in which signals originating at the ECM could, in turn, regulate the deposition of ECM components by controlling the levels of SEC23A, while SEC23B would respond to growth factor related cues, a scenario which would explain the lack of common functional interactors in our screen.

Finally, the ECM-mediated regulation of SEC23A might also be relevant for cancer. It has been shown that downregulation of SEC23A leads to changes in the secretome of cancer cells that promote metastatic capabilities (Korpal et al. 2011; Szczyrba et al. 2011). As metastatic cancer cells migrate and interact dynamically with the ECM it is plausible that signals arising from the ECM contribute to SEC23A regulation in

cancer cells, although this needs further investigation.

MATERIALS AND METHODS

Cell lines and reagents.

HeLa Kyoto cells were a gift from Shuh Narumiya (Kyoto University) and were cultured in DMEM supplemented with 10% FCS and 2 mM glutamine. Normal human primary lung fibroblasts were obtained from Lonza (Basel, Switzerland) and were cultured in fibroblast growth basal medium. HeLa cells stably expressing P24-YFP (TMED2) were generated in house and describe before (Simpson, Nilsson, and Pepperkok 2006). All cells were kept in a humidified incubator at 37ºC and 5% CO_2.

All siRNAs used were from Ambion and are described in **Table 1.** Anti VSVG antibody and recombinant adenovirus expressing YFP-tagged tsO45G thermosensitive version of VSVG were a gift from Kai Simmons (MPI-CBG, Dresden, Germany). Large scale adenovirus preparation was done by Vector Biolabs. RUSH construct encoding E-Cadherin-GFP was a gift from Frank Perez (Institute Curie, Paris, France). Anti MACF1 antibody was a gift from Ronald Liem (Columbia University, NY, USA). The following primary antibodies were used: SEC23A (ab179811) from Abcam, Vinculin (MAB3574) from Merck, EEA1 (610457) and GM130 (610822) from BD biosciences, Alpha-Tubulin (MS581P1) from Thermo Fisher, SEC23B (GTX82432) from GeneTex, GFP (11814460001) from Roche. Anti-beta COPI rabbit serum was produced in house. The following secondary antibodies were used: rabbit anti mouse-HRP (A9044) from Merck, goat anti rabbit-HRP (ab6721) from Abcam and Alexa-conjugated antibodies from Molecular probes. FAK inhibitor PND-1186 was from Tocris Bioscience. Matrigel was from Corning. Cycloheximide was from Calbiochem, Biotin was from Sigma.

siRNA-based functional interaction screen

The cytoskeleton siRNA library was designed in house and contains 848 siRNAs targeting 378 cytoskeleton, associated and regulatory proteins (**Table 1**). The cytoskeleton siRNAs were spotted on Nunc Lab-Tek chambers at a density of 384 spots per chamber as previously described (Simpson et al. 2012). The whole cytoskeleton library was distributed on 4 Lab-Tek chambers which included also positive controls (beta and gamma *COPI* targeting siRNAs), 2 different non-targeting siRNAs (Scramble and Neg9 siRNAs) and an *INCENP* targeting siRNA to evaluate the transfection efficiency of the plate based on the number of multinucleated cells (Neumann et al. 2006). Spotted Lab-Teks were dried, stored in humidity-free containers and used within a month after coating. At the moment of cell plating, cells were transfected either with *SEC23A*, *SEC23B*, or control siRNAs in suspension at a final concentration of 15 nM using Lipofectamine 2000 and Opti-MEM (Thermo Fisher) according to the manufacturer's instructions. 1.5 mL of transfected cell suspension containing 100,000 cells were plated onto each Lab-Tek. At 48 hrs after plating, cells were infected with adenovirus coding for the VSVG-tsO45-YFP protein (henceforth called VSVG-YFP) for 1 hr at 37ºC, washed twice and transferred to 40ºC for 15 hrs to accumulate VSVG-YFP in the ER as described (see Simpson et al., 2012). Release of the transport marker from the ER was induced by shifting temperature to 32ºC in fresh DMEM containing 25 mM HEPES and 50 µg/mL of cycloheximide. After 1 hr at 32ºC cells were washed twice with PBS and fixed with PFA 3% for 20 min. VSVG at the plasma membrane was detected by incubating cells for 1h with an anti-VSVG antibody (1:100) recognizing an extracellular epitope of VSVG, followed by 30 min incubation of anti-mouse Alexa-647 secondary antibody (1:500). Cell nuclei were stained with Hoechst dye 33258. Finally, cells were washed twice with PBS and left with PBS for imaging. Images

were acquired on an Olympus ScanR microscope using a 20X/0.7 NA objective. The whole screen was carried out in 5 independent biological replicas.

Images were analyzed using CellProfiler (Carpenter et al. 2006) as previously described (Scharaw et al. 2016). For the analysis, only images with a number of cells between 5-200 were considered. The transport ratio per cell was defined as the VSVG specific intensity at the plasma membrane (A647 signal) divided by the VSVG-YFP intensity (representing the total cellular amount of VSVG expressed). Transport ratios for each siRNA were converted to transport scores according to the following formula: Transport score = $xi - X/MAD$ where xi is the average transport ratio per cell for the siRNA of interest, X is determined as the median of 25 (5x5 matrix) transport ratios from neighbouring siRNA sports surrounding the siRNA spot of interest. MAD is the median absolute deviation in the 5x5 matrix. (**Table 2**).

Based on our positive controls (*COPB1, COPG1, SEC23A/B*) we set our threshold on a transport score of -1.5 (strong inhibition). By symmetry, only combinations showing scores above 1.5 were considered as transport accelerators. Both non-targeting siRNAs (Scramble and Neg9) had transport scores close to 0 (0.08 and -0.16 respectively) so we selected Neg9 as a control siRNA for our following analysis. As quality control, we only considered the plates in which our positive controls showed strong transport inhibition and the negatives controls had a score close very close to 0. Finally, we considered only the siRNAs for which we had at least 3 biological replicas and we computed the median transport score for each siRNA. To obtain the hits, we compared the added median transport scores of the single knockdowns vs the double knockdowns and selected the ones in which the difference was greater than 1 transport score unit (**Table 2** and Table legends).

RUSH assay

For the RUSH assay the cells were plated in coverslips in 24-well plates at a density of 15,000 cells per well and 24 hrs later transfected with siRNAs using Lipofectamine 2000 and serum-free DMEM. 24 hrs later the cells were transfected with the RUSH construct encoding E-cadherin using Lipofectamine LTX and Enhancer in serum-free DMEM (as per manufacturer´s instructions). The next day the RUSH assay was performed as described previously (Boncompain et al. 2012). In brief, cell medium was changed to fresh DMEM containing 40 µM biotin and 50 µg/mL of cycloheximide. After 45 min cells were washed once with ice-cold PBS and incubated with anti-GFP (1:100) in PBS on ice for 45 min. After incubation, cells were washed twice with PBS and fixed with PFA 3% at room temperature for 20 min. After washing two times with PBS cells were stained for 30 min with an anti-mouse Alexa-647 antibody (1:500). Cell nuclei were stained with Hoechst dye 33258. Finally, coverslips were mounted on glass slides using Mowiol mounting media and images where acquired and analyzed with CellProfiler as above. For every condition, a non-release control was also included to account for cargo leakiness.

Confocal microscopy and image segmentation

Confocal stacks were acquired using a Leica SP8 system with a 63X/1.4 NA objective and Zeiss 780 with a 40X/1.1 NA objective. Unless otherwise stated, the images shown represent maximum intensity Z-projections. Pipelines for quantification of ERES, COPI transport intermediates and focal adhesions were implemented as custom Fiji plugins. ERES and COPI structures were segmented and quantified in 3D in the individual cells using functions of the 3D image suite library (Ollion et al. 2013). First nuclei were segmented in Hoechst channel. Cell masks were identified by applying watershed algorithm in the COPI channel using previously segmented nuclei as seeds. For robust segmentation of ERES and COPI positive structures, 3D median

filters were applied for noise suppression and for subtracting local background in corresponding channels. Seeds for the potential structures were identified by applying local maximum filter. Individual structures were segmented using spot segmentation plugin of 3D image suite including watershed separation of touching structures. When processing the COPI channel, big positive clusters, which presumably correspond to the Golgi complex, were segmented in 3D by thresholding and excluded from spot analysis. Pipeline documented the number of identified structures in each cell, their integrated intensity and the integrated intensity of entire cell.

The optical plane where focal adhesions are located was identified as the optical slice with the largest normalised variance. Segmentation of focal adhesions was performed in 2D by thresholding on the maximum Z-projections of 3 confocal slices centred on the identified plane to exclude cytoplasmic staining in other planes from the analysis. Total area of focal adhesions in each image was quantified. Nuclei were segmented in Hoechst channel to normalise the area of focal adhesions to the number of cells.

Electron microscopy

Cell monolayers were fixed in 2.5% glutaraldehyde in cacodylate buffer, washed with cacodylate and post-fixed in 1% osmium. En-bloc staining was done in 1% uranyl acetate (UA). The cells were then dehydrated in ethanol, and embedded in Epon resin. All specimen preparation steps up to embedding were done using a PELCO Biowave Pro microwave (Lorentzen et al. 2018). Thin sections of 70 nm were collected in 2x1 slot grids and post stained with lead citrate. The imaging was done using LLP viewer in a JEOL 2200 Plus electron microscope equipped with a Matataki camera.

RT-qPCR

Total RNA was extracted using RNAeasy kit (Qiagen). 500 µg of total RNA was subjected to reverse transcription using SuperScript III First Strand Synthesis Supermix (Invitrogen) according to manufacturer´s instructions. cDNAs obtained this way was diluted 1/10 and used for PCR. The RT-qPCR reaction was performed using the SYBR green detection reagent (Applied Biosystems) in StepOne Real-Time PCR System machines using the StepOne software v2.3 (Applied Biosystems). Primer sequences are described in the supplementary information. Changes in gene expression were calculated with the $2^{-\Delta\Delta CT}$ method (Livak and Schmittgen 2001) using *GAPDH* as the housekeeping gene.

mRNA-Seq

Individually barcoded stranded mRNA-Seq libraries were prepared from high-quality total RNA samples (~600 ng/sample) using the Illumina TruSeq RNA Sample Preparation v2 Kit (Illumina) implemented on the liquid handling robot Beckman FXP2. Obtained libraries that passed the QC step were pooled in equimolar amounts; 1.8 pM solution of this pool was loaded on the Illumina sequencer NextSeq 500 and sequenced uni-directionally, generating ~500 million reads, each 85 bases long.

Single-end sequencing reads were aligned to the human genome (version GRCh38) and the reference gene annotation (release 84, Ensembl) using STAR v2.6.0a (Dobin et al. 2013) with default parameters. Read counts per gene matrices were generated during the alignment step (--quantMode GeneCounts). Gene counts were then compared between 2 groups of replicated samples using the DESeq R package (Love, Huber, and Anders 2014). Differentially expressed genes were selected based on their p-adjusted value lower than 10% and their Log2 fold change above 0.58 or below -0.58

ECM experiments

For preparing ECM derived from lung fibroblasts, cells were seeded at a density of 20,000-25,000 cells/well in 24 glass-bottom well plates. After 18 hrs cells were switched to DMEM medium with macromolecular crowding (a mixture of Ficol 70 and Ficol 400). Cells were cultured for 5 days with stimulation (TGFß1 5 ng/ml) and media change on day 1 and day 4. On day 5, cells were washed with PBS and the plates were subjected to decellularization using 1% Triton.

Co-immunoprecipitation and Western Blot analysis

For Co-IP experiments, Hela cells were plated on a 10 cm Petri dish and lysed at approximately 90% of confluency using NP-40 lysis buffer (1% NP-40, 150 mM NaCl, 50 mM Tris/HCl pH 7.4) supplemented with protease inhibitors. All subsequent steps were carried out at 4ºC. Cells were lysed for 30 min and centrifuged at 20,000 g for 15 min. 60 µL of protein G-agarose were added to 400 µL of lysate in the presence or absence of 2 µg of anti-MACF1 antibody and incubated with rotation overnight. Beads were pelleted and washed 3 times with lysis buffer and then heated at 60ºC for 5 min with sample buffer 2x (10% glycerol, 4.5% SDS, 130 mM DDT, 0.005% bromophenol blue, 80 mM Tris/HCl pH 6.8). Proteins were separated by SDS-PAGE using a 3-8% Tris-Acetate gel and then transferred to PVDF membranes for Western blotting.

For SEC23A experiments, cells were plated in 12 well plates, treated with the respective siRNAs for 48 hrs and then lysed directly with sample buffer 2x. Lysates were treated with Benzonase for 10 min at room temperature and then heated at 90ºC for 5 min. Proteins were separated by SDS-PAGE using a 4-12% Bis-Tris gel and transferred to PVDF membranes as above.

TABLE INFORMATION

Table 1. Cytoskeleton siRNA library and other siRNAs

All siRNA used are predesigned Silencer Select from Ambion except otherwise stated. They were selected based on score and number of transcripts targeted.

Table 2. Screen results

The first column, “spotted siRNA”, refers to the cytoskeleton library. The second column refers to the siRNAs transfected in liquid suspension. The third column shows the median value of all the biological replicas for a given combination. The results shown here include only the plates that passed quality control.

Table 3. SEC23 interactors

The top 25 double knockdown combinations are listed according to transport scores. The expected additive effects refers to the expected transport score if the siRNA perturbations would have an additive effect. (Observed – expected) refers to the transport score difference between the observed score in the double knockdown minus the expected score assuming additive effect.

The flagged combinations were not considered. The flags are the following:

1) Value in single knockdown is too high (>0.75 or <-0.75), 2) Difference between observed and expected transport scores is less than 1 transport score unit, 3) Gene not expressed in HeLa cells (according to our own transcriptomic analysis), 4) Less than 3 biological replicas, 5) Transport score in double knockdown below the 1.5 threshold, 6) siRNA does not target the specified gene in current Ensembl version GRCh38.

Table 4. Differential expression analysis

The differential expression analysis was set at -0.58>Log2FC >0.58 and the p-adjusted at 0.1. The values listed correspond to individual knockdowns compared to the control non-targeting siRNA

Table 5. Secretory pathway related genes

Differential expression analysis for a set of 595 annotated and manually curated secretory pathway genes based on a list previously published (Feizi et al. 2017)

Table 6. Gene enrichment

Top 50 GO: biological processes ranked by the number of genes for each knockdown. Enrichment value was set at a minimum of 1.5 and the p-value at 0.01.

ACKNLOWLEDGMENTS:

We would like to thank the EMBL Advanced Light Microscopy Facility for help with the preparation and analysis of the screen, the EMBL Genomics Core Facility for help with mRNA-Seq sample preparation and analysis, Seetharaman Parashuraman (Institute of Biochemistry and Cell Biology, Naples, Italy) for useful discussions and critical reading of the manuscript, and members of the Pepperkok Team for fruitful discussions during the development of this project. JJ was funded by a Fellowship from National Commission for Scientific and Technological Research, Chile. MMK was funded by a BMBF grant (German Centre for Lung Research, DZL).

AUTHOR CONTRIBUTION:

Conceptualization: Juan Jung, Rainer Pepperkok, Muzamil M. Khan
Investigation: Juan Jung, Muzamil M. Khan
Formal Analysis: Juan Jung, Muzamil M. Khan, Jonathan Landry, Aliaksandr Halavatyi
Resources: Pedro Machado, Miriam Reiss
Supervision: Rainer Pepperkok
Writing original draft: Juan Jung, Rainer Pepperkok, Muzamil M. Khan
Writing review and editing: all the authors
Funding acquisition Rainer Pepperkok, Juan Jung

REFERENCES

Amano, Mutsuki, Kazuyasu Chihara, Kazushi Kimura, Yuko Fukata, Nao Nakamura, Yoshiharu Matsuura, and Kozo Kaibuchi. 1997. “Formation of Actin Stress Fibers and Focal Adhesions Enhanced by Rho-Kinase.” *Science* 275 (5304): 1308–11. https://doi.org/10.1126/science.275.5304.1308.

Anitei, Mihaela, and Bernard Hoflack. 2012. “Bridging Membrane and Cytoskeleton Dynamics in the Secretory and Endocytic Pathways.” *Nature Publishing Group* 14 (1). https://doi.org/10.1038/ncb2409.

Bard, Frederic, Laetitia Casano, Arrate Mallabiabarrena, Erin Wallace, Kota Saito, Hitoshi Kitayama, Gianni Guizzunti, et al. 2006. “Functional Genomics Reveals Genes Involved in Protein Secretion and Golgi Organization.” *Nature* 439 (7076): 604–7. https://doi.org/10.1038/nature04377.

Binder, Janos X., Sune Pletscher-Frankild, Kalliopi Tsafou, Christian Stolte, Seán I. O’Donoghue, Reinhard Schneider, and Lars Juhl Jensen. 2014. “COMPARTMENTS: Unification and Visualization of Protein

Subcellular Localization Evidence." *Database* 2014: 1–9. https://doi.org/10.1093/database/bau012.

Boncompain, Gaelle, Severine Divoux, Nelly Gareil, Helene de Forges, Aurianne Lescure, Lynda Latreche, Valentina Mercanti, Florence Jollivet, Graça Raposo, and Franck Perez. 2012. "Synchronization of Secretory Protein Traffic in Populations of Cells." *Nature Methods* 9 (5): 493–98. https://doi.org/10.1038/nmeth.1928.

Boyadjiev, Simeon A., J. Christopher Fromme, Jin Ben, Samuel S. Chong, Christopher Nauta, David J. Hur, George Zhang, et al. 2006. "Cranio-Lenticulo-Sutural Dysplasia Is Caused by a SEC23A Mutation Leading to Abnormal Endoplasmic-Reticulum-to-Golgi Trafficking." *Nature Genetics* 38 (10): 1192–97. https://doi.org/10.1038/ng1876.

Burgo, Andrea, Véronique Proux-Gillardeaux, Emmanuel Sotirakis, Philippe Bun, Alessandra Casano, Agathe Verraes, Ronald K H Liem, Etienne Formstecher, Maïté Coppey-Moisan, and Thierry Galli. 2012. "A Molecular Network for the Transport of the TI-VAMP/VAMP7 Vesicles from Cell Center to Periphery." *Developmental Cell* 23 (1): 166–80. https://doi.org/10.1016/j.devcel.2012.04.019.

Carpenter, Anne E., Thouis R. Jones, Michael R. Lamprecht, Colin Clarke, In Han Kang, Ola Friman, David A. Guertin, et al. 2006. "CellProfiler: Image Analysis Software for Identifying and Quantifying Cell Phenotypes." *Genome Biology* 7 (10). https://doi.org/10.1186/gb-2006-7-10-r100.

Dobin, Alexander, Carrie A. Davis, Felix Schlesinger, Jorg Drenkow, Chris Zaleski, Sonali Jha, Philippe Batut, Mark Chaisson, and Thomas R. Gingeras. 2013. "STAR: Ultrafast Universal RNA-Seq Aligner." *Bioinformatics* 29 (1): 15–21. https://doi.org/10.1093/bioinformatics/bts635.

Eisler, Stephan A., Filipa Curado, Gisela Link, Sarah Schulz, Melanie Noack, Maren Steinke, Monilola A. Olayioye, and Angelika Hausser. 2018. "A Rho Signaling Network Links Microtubules to PKD Controlled Carrier Transport to Focal Adhesions." *ELife* 7: 1–30. https://doi.org/10.7554/eLife.35907.

Farhan, Hesso, Markus W Wendeler, Sandra Mitrovic, Eugenio Fava, Yael Silberberg, Roded Sharan, Marino Zerial, and Hans-Peter Hauri. 2010. "MAPK Signaling to the Early Secretory Pathway Revealed by Kinase/Phosphatase Functional Screening." *The Journal of Cell Biology* 189 (6): 997–1011. https://doi.org/10.1083/jcb.200912082.

Feizi, Amir, Francesco Gatto, Mathias Uhlen, and Jens Nielsen. 2017. "Human Protein Secretory Pathway Genes Are Expressed in a Tissue-Specific Pattern to Match Processing Demands of the Secretome." *Npj Systems Biology and Applications* 3 (1): 1–9. https://doi.org/10.1038/s41540-017-0021-4.

Fourriere, Lou, Ana Joaquina Jimenez, Franck Perez, and Gaelle Boncompain. 2020. "The Role of Microtubules in Secretory Protein Transport." *Journal of Cell Science* 133 (2). https://doi.org/10.1242/jcs.237016.

Fujiwara, T., K. Oda, S. Yokota, A. Takatsuki, and Y. Ikehara. 1988. "Brefeldin A Causes Disassembly of the Golgi Complex and Accumulation of Secretory Proteins in the Endoplasmic Reticulum." *Journal of Biological Chemistry* 263 (34): 18545–52. https://doi.org/10.1016/s0021-9258(19)81393-5.

Geiger, Benjamin, Joachim P. Spatz, and Alexander D. Bershadsky. 2009. "Environmental Sensing through Focal Adhesions." *Nature Reviews Molecular Cell Biology* 10 (1): 21–33. https://doi.org/10.1038/nrm2593.

Gurel, Pinar S, Anna L Hatch, and Henry N Higgs. 2014. "Connecting the Cytoskeleton to the Endoplasmic Reticulum and Golgi," 660–72. https://doi.org/10.1016/j.cub.2014.05.033.

Janmey, Paul A. 1998. "The Cytoskeleton and Cell Signaling: Component Localization and Mechanical Coupling." *Physiological Reviews* 78 (3): 763–81. https://doi.org/10.1152/physrev.1998.78.3.763.

Kakinuma, Takumi, Haruo Ichikawa, Yoshito Tsukada, Takashi Nakamura, and Ban Hock Toh. 2004. "Interaction between P230 and MACF1 Is Associated with Transport of a Glycosyl Phosphatidyl Inositol-

Anchored Protein from the Golgi to the Cell Periphery." *Experimental Cell Research* 298 (2): 388–98. https://doi.org/10.1016/j.yexcr.2004.04.047.

Karakesisoglou, Iakowos, Yanmin Yang, and Elaine Fuchs. 2000. "An Epidermal Plakin That Integrates Actin and Microtubule Networks at Cellular Junctions." *Journal of Cell Biology* 149 (1): 195–208. https://doi.org/10.1083/jcb.149.1.195.

Khoriaty, Rami, Lesley Everett, Jennifer Chase, Guojing Zhu, Mark Hoenerhoff, Brooke Mcknight, Matthew P Vasievich, Bin Zhang, Kärt Tomberg, and John Williams. 2016. "Pancreatic SEC23B Deficiency Is Sufficient to Explain the Perinatal Lethality of Germline SEC23B Deficiency in Mice." *Nature Publishing Group*, no. June: 1–10. https://doi.org/10.1038/srep27802.

Khoriaty, Rami, Geoffrey G. Hesketh, Amélie Bernard, Angela C. Weyand, Dattatreya Mellacheruvu, Guojing Zhu, Mark J. Hoenerhoff, et al. 2018. "Functions of the COPII Gene Paralogs SEC23A and SEC23B Are Interchangeable in Vivo." *Proceedings of the National Academy of Sciences of the United States of America* 115 (33): E7748–57. https://doi.org/10.1073/pnas.1805784115.

Khoriaty, Rami, Nancy Vogel, Mark J Hoenerhoff, M Dolors Sans, Guojing Zhu, and Thomas F J Martin. 2017. "SEC23B Is Required for Pancreatic Acinar Cell Function in Adult Mice." https://doi.org/10.1091/mbc.E17-01-0001.

Korpal, Manav, Brian J. Ell, Francesca M. Buffa, Toni Ibrahim, Mario A. Blanco, Toni Celià-Terrassa, Laura Mercatali, et al. 2011. "Direct Targeting of Sec23a by MiR-200s Influences Cancer Cell Secretome and Promotes Metastatic Colonization." *Nature Medicine* 17 (9): 1101–9. https://doi.org/10.1038/nm.2401.

Kreis, Thomas E., and Harvey F. Lodish. 1986. "Oligomerization Is Essential for Transport of Vesicular Stomatitis Viral Glycoprotein to the Cell Surface." *Cell* 46 (6): 929–37. https://doi.org/10.1016/0092-8674(86)90075-9.

Lang, Michael R., Lynne A. Lapierre, Michael Frotscher, James R. Goldenring, and Ela W. Knapik. 2006. "Secretory COPII Coat Component Sec23a Is Essential for Craniofacial Chondrocyte Maturation." *Nature Genetics* 38 (10): 1198–1203. https://doi.org/10.1038/ng1880.

Laufer, Christina, Bernd Fischer, Maximilian Billmann, Wolfgang Huber, and Michael Boutros. 2013. "Mapping Genetic Interactions in Human Cancer Cells with RNAi and Multiparametric Phenotyping." *Nature Methods* 10 (5): 427–31. https://doi.org/10.1038/nmeth.2436.

Leung, Conrad L., Dongming Sun, Min Zheng, David R. Knowles, and Ronald K.H. Liem. 1999. "Microtubule Actin Cross-Linking Factor (MACF): A Hybrid of Dystonin and Dystrophin That Can Interact with the Actin and Microtubule Cytoskeletons." *Journal of Cell Biology* 147 (6): 1275–85. https://doi.org/10.1083/jcb.147.6.1275.

Lin, Chung-Ming, Hui-Jye Chen, Conrad L Leung, David a D Parry, and Ronald K H Liem. 2005. "Microtubule Actin Crosslinking Factor 1b: A Novel Plakin That Localizes to the Golgi Complex." *Journal of Cell Science* 118 (Pt 16): 3727–38. https://doi.org/10.1242/jcs.02510.

Liu, Lin, Jie Cai, Huimin Wang, Xijun Liang, Qian Zhou, Chenyun Ding, Yuangang Zhu, et al. 2019. "Coupling of COPII Vesicle Trafficking to Nutrient Availability by the IRE1α-XBP1s Axis." *Proceedings of the National Academy of Sciences of the United States of America* 116 (24): 11776–85. https://doi.org/10.1073/pnas.1814480116.

Livak, Kenneth J., and Thomas D. Schmittgen. 2001. "Analysis of Relative Gene Expression Data Using Real-Time Quantitative PCR and the 2-ΔΔCT Method." *Methods* 25 (4): 402–8. https://doi.org/10.1006/meth.2001.1262.

Lorentzen, Anna, Paul F. Becker, Jan Kosla, Massimo Saini, Kathrin Weidele, Paolo Ronchi, Corinna Klein, et

al. 2018. “Single Cell Polarity in Liquid Phase Facilitates Tumour Metastasis.” *Nature Communications* 9 (1). https://doi.org/10.1038/s41467-018-03139-6.

Love, Michael I., Wolfgang Huber, and Simon Anders. 2014. “Moderated Estimation of Fold Change and Dispersion for RNA-Seq Data with DESeq2.” *Genome Biology* 15 (12): 1–21. https://doi.org/10.1186/s13059-014-0550-8.

Matteis, Maria Antonietta De, and Alberto Luini. 2011. “Mendelian Disorders of Membrane Trafficking.” *The New England Journal of Medicine* 365 (10): 927–38. https://doi.org/10.1056/NEJMra0910494.

Miller, Elizabeth A., and Randy Schekman. 2013. “COPII - a Flexible Vesicle Formation System.” *Current Opinion in Cell Biology* 25 (4): 420–27. https://doi.org/10.1016/j.ceb.2013.04.005.

Montanez, Eloi, Siegfried Ussar, Martina Schifferer, Michael Bösl, Roy Zent, Markus Moser, and Reinhard Fässler. 2008. “Kindlin-2 Controls Bidirectional Signaling of Integrins.” *Genes and Development* 22 (10): 1325–30. https://doi.org/10.1101/gad.469408.

Moujaber, Ossama, and Ursula Stochaj. 2019. “The Cytoskeleton as Regulator of Cell Signaling Pathways.” *Trends in Biochemical Sciences*, 1–12. https://doi.org/10.1016/j.tibs.2019.11.003.

Neumann, Beate, Michael Held, Urban Liebel, Holger Erfle, Phill Rogers, Rainer Pepperkok, and Jan Ellenberg. 2006. “High-Throughput RNAi Screening by Time-Lapse Imaging of Live Human Cells.” *Nature Methods* 3 (5): 385–90. https://doi.org/10.1038/nmeth876.

Nolte, Martijn A, Esther N M Nolte- Hoen, and Coert Margadant. 2020. “Trends in Biochemical Sciences Integrins Control Vesicular Traf Fi Cking ; New Tricks for Old Dogs.” *Trends in Biochemical Sciences*, 1–14. https://doi.org/10.1016/j.tibs.2020.09.001.

Ollion, Jean, Julien Cochennec, François Loll, Christophe Escudé, and Thomas Boudier. 2013. “TANGO: A Generic Tool for High-Throughput 3D Image Analysis for Studying Nuclear Organization.” *Bioinformatics* 29 (14): 1840–41. https://doi.org/10.1093/bioinformatics/btt276.

Presley, J F, N B Cole, T a Schroer, K Hirschberg, K J Zaal, and J Lippincott-Schwartz. 1997. “ER-to-Golgi Transport Visualized in Living Cells.” *Nature* 389 (6646): 81–85. https://doi.org/10.1038/38001.

Roguev, Talbot, Negri, Shales, Cagney, Bandyopadhyay, Panning, and Krogan. 2013. “Quantitative Genetic-Interaction Mapping in Mammalian Cells.” *Nature Methods* 10 (5): 432–37. https://doi.org/10.1038/nmeth.2398.

Scales, Suzie J., Rainer Pepperkok, and Thomas E. Kreis. 1997. “Visualization of ER-to-Golgi Transport in Living Cells Reveals a Sequential Mode of Action for COPII and COPI.” *Cell* 90 (6): 1137–48. https://doi.org/10.1016/S0092-8674(00)80379-7.

Scharaw, Sandra, Murat Iskar, Alessandro Ori, Gaelle Boncompain, Vibor Laketa, Ina Poser, Emma Lundberg, et al. 2016. “The Endosomal Transcriptional Regulator RNF11 Integrates Degradation and Transport of EGFR.” *Journal of Cell Biology* 215 (4): 543–58. https://doi.org/10.1083/jcb.201601090.

Simpson, Jeremy C., Tommy Nilsson, and Rainer Pepperkok. 2006. “Biogenesis of Tubular ER-to-Golgi Transport Intermediates.” *Molecular Biology of the Cell* 17 (2): 723–37. https://doi.org/10.1091/mbc.e05-06-0580.

Simpson, Jeremy C, Brigitte Joggerst, Vibor Laketa, Fatima Verissimo, Cihan Cetin, Holger Erfle, Mariana G Bexiga, et al. 2012. “Genome-Wide RNAi Screening Identifies Human Proteins with a Regulatory Function in the Early Secretory Pathway.” *Nature Cell Biology* 14 (7): 1–13. https://doi.org/10.1038/ncb2510.

Stehbens, Samantha J., Matthew Paszek, Hayley Pemble, Andreas Ettinger, Sarah Gierke, and Torsten Wittmann. 2014. “CLASPs Link Focal-Adhesion-Associated Microtubule Capture to Localized Exocytosis

and Adhesion Site Turnover." *Nature Cell Biology* 16 (6): 558–70. https://doi.org/10.1038/ncb2975.

Sun, Zhiqi, Shengzhen S Guo, and Reinhard Fässler. 2016. "Integrin-Mediated Mechanotransduction" 215 (4).

Szczyrba, Jaroslaw, Elke Nolte, Sven Wach, Elisabeth Kremmer, Robert Stöhr, Arndt Hartmann, Wolf Wieland, Bernd Wullich, and Friedrich A. Grässer. 2011. "Downregulation of Sec23A Protein by MiRNA-375 in Prostate Carcinoma." *Molecular Cancer Research* 9 (6): 791–800. https://doi.org/10.1158/1541-7786.MCR-10-0573.

Szklarczyk, Damian, Annika L. Gable, David Lyon, Alexander Junge, Stefan Wyder, Jaime Huerta-Cepas, Milan Simonovic, et al. 2019. "STRING V11: Protein-Protein Association Networks with Increased Coverage, Supporting Functional Discovery in Genome-Wide Experimental Datasets." *Nucleic Acids Research* 47 (D1): D607–13. https://doi.org/10.1093/nar/gky1131.

Thul, Peter J., Lovisa Akesson, Mikaela Wiking, Diana Mahdessian, Aikaterini Geladaki, Hammou Ait Blal, Tove Alm, et al. 2017. "A Subcellular Map of the Human Proteome." *Science* 356 (6340). https://doi.org/10.1126/science.aal3321.

Tillmann, Kerstin D., Veronika Reiterer, Francesco Baschieri, Julia Hoffmann, Valentina Millarte, Mark A. Hauser, Arnon Mazza, et al. 2015. "Regulation of Sec16 Levels and Dynamics Links Proliferation and Secretion." *Journal of Cell Science* 128 (4): 670–82. https://doi.org/10.1242/jcs.157115.

Tu, Yizeng, Shan Wu, Xiaohua Shi, Ka Chen, and Chuanyue Wu. 2003. "Migfilin and Mig-2 Link Focal Adhesions to Filamin and the Actin Cytoskeleton and Function in Cell Shape Modulation." *Cell* 113 (1): 37–47. https://doi.org/10.1016/S0092-8674(03)00163-6.

Verissimo, Fatima, Aliaksandr Halavatyi, Rainer Pepperkok, and Matthias Weiss. 2015. "A Microtubule-Independent Role of P150glued in Secretory Cargo Concentration at Endoplasmic Reticulum Exit Sites." *Journal of Cell Science* 49 (October): 4160–70. https://doi.org/10.1242/jcs.172395.

Watson, Peter, Rebecca Forster, Krysten J Palmer, Rainer Pepperkok, and David J Stephens. 2005. "Coupling of ER Exit to Microtubules through Direct Interaction of COPII with Dynactin." *Nature Cell Biology* 7 (1): 48–55. https://doi.org/10.1038/ncb1206.

Wickström, Sara A., and Reinhard Fässler. 2011. "Regulation of Membrane Traffic by Integrin Signaling." *Trends in Cell Biology* 21 (5): 266–73. https://doi.org/10.1016/j.tcb.2011.02.003.

Wu, Xiaoyang, Atsuko Kodama, and Elaine Fuchs. 2008. "ACF7 Regulates Cytoskeletal-Focal Adhesion Dynamics and Migration and Has ATPase Activity." *Cell* 135 (1): 137–48. https://doi.org/10.1016/j.cell.2008.07.045.

Yarwood, Rebecca, John Hellicar, Philip G. Woodman, and Martin Lowe. 2020. "Membrane Trafficking in Health and Disease." *DMM Disease Models and Mechanisms* 13 (4). https://doi.org/10.1242/dmm.043448.

Zacharogianni, Margarita, Vangelis Kondylis, Yang Tang, Hesso Farhan, Despina Xanthakis, Florian Fuchs, Michael Boutros, and Catherine Rabouille. 2011. "ERK7 Is a Negative Regulator of Protein Secretion in Response to Amino-Acid Starvation by Modulating Sec16 Membrane Association." *EMBO Journal* 30 (18): 3684–3700. https://doi.org/10.1038/emboj.2011.253.

Zaidel-Bar, Ronen, Shalev Itzkovitz, Avi Ma'ayan, Ravi Iyengar, and Benjamin Geiger. 2007. "Functional Atlas of the Integrin Adhesome." *Nature Cell Biology* 9 (8): 858–67. https://doi.org/10.1038/ncb0807-858.

Zhang, Chun Jiang, Anne G. Rosenwald, Mark C. Willingham, Susan Skuntz, Jenny Clark, and Richard A. Kahn. 1994. "Expression of a Dominant Allele of Human ARF1 Inhibits Membrane Traffic in Vivo." *Journal of Cell Biology* 124 (3): 289–300. https://doi.org/10.1083/jcb.124.3.289.

Zhou, Yingyao, Bin Zhou, Lars Pache, Max Chang, Alireza Hadj Khodabakhshi, Olga Tanaseichuk,

Christopher Benner, and Sumit K. Chanda. 2019. “Metascape Provides a Biologist-Oriented Resource for the Analysis of Systems-Level Datasets.” *Nature Communications* 10 (1). https://doi.org/10.1038/s41467-019-09234-6.

SUPPLEMENTARY FIGURES

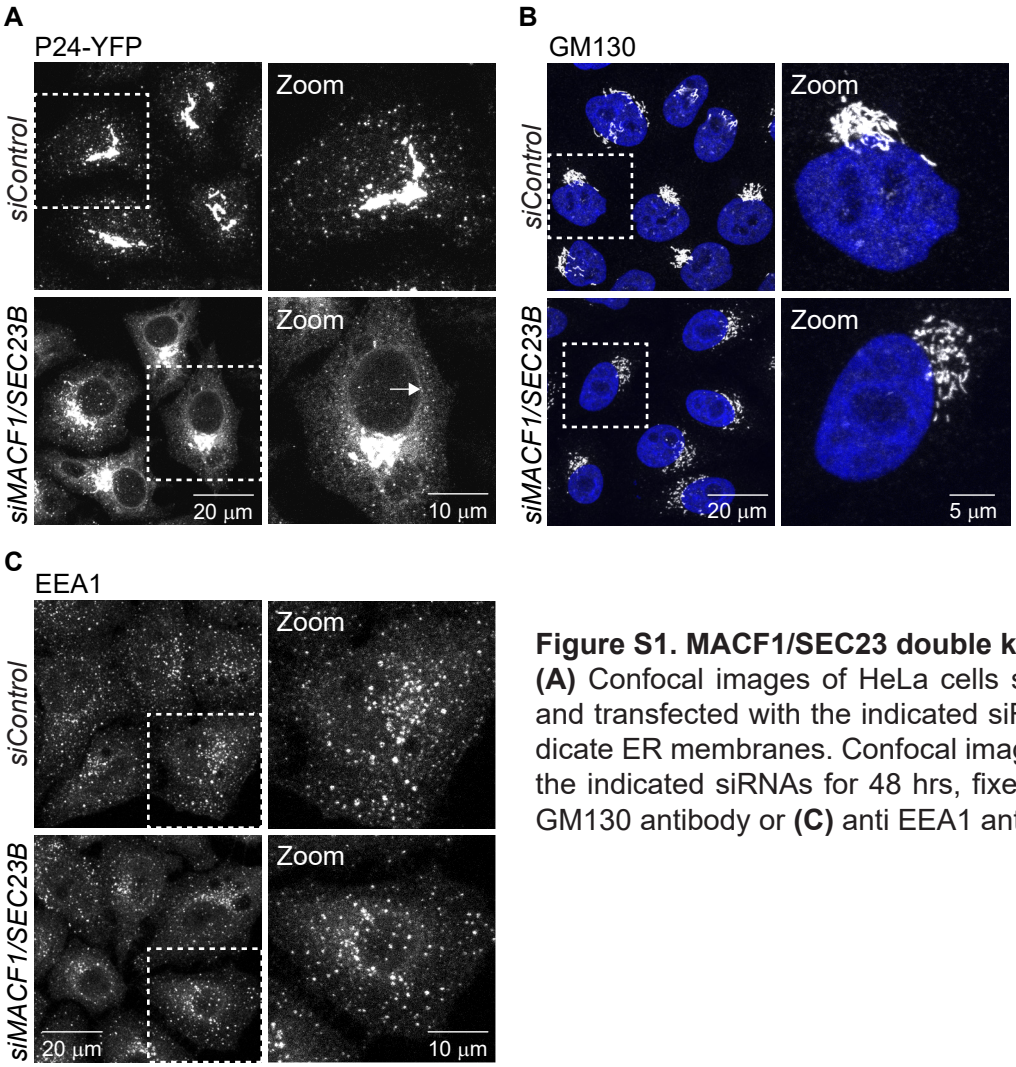

Figure S1. MACF1/SEC23 double knockdown affects ER exit
(A) Confocal images of HeLa cells stably expressing P24-YFP and transfected with the indicated siRNAs for 48 hrs. Arrows indicate ER membranes. Confocal images of cells transfected with the indicated siRNAs for 48 hrs, fixed and stained with **(B)** anti GM130 antibody or **(C)** anti EEA1 antibody.

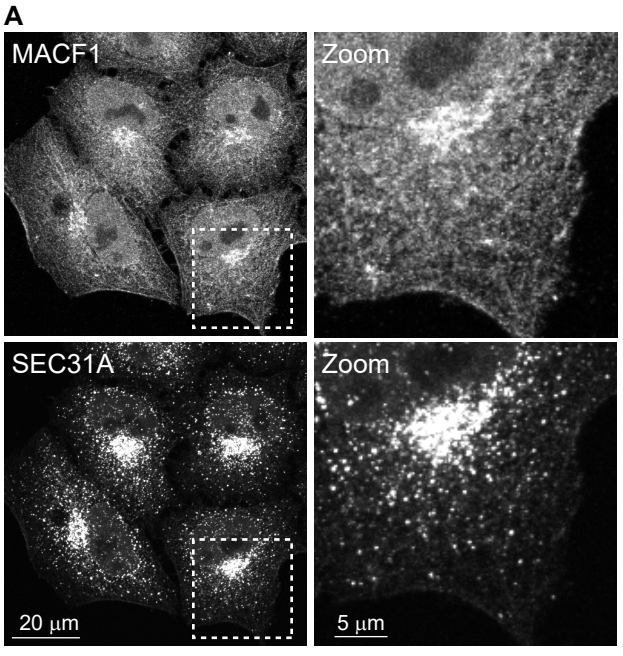

Figure S2. MACF1 and SEC23B do not interact physically
(A) Confocal images of untreated HeLa cells fixed and co-stained for MACF1 and SEC31A as a marker for ERES. **(B)** Co-IP experiment. HeLa cells were lysed and incubated with anti MACF1 antibody bound to agarose-protein G beads at 4°C overnight. The beads were washed and loaded into gels. Western-Blot was performed using anti MACF1 and anti SEC23B antibodies.

A

Knock down	DE genes	Down	Up
CRKL	601	368	233
FERMT2	589	317	272
MACF1	244	156	88
MAPK8IP2	374	301	73
NGEF	205	140	65
PIK3CA	999	419	580
ROCK1	105	100	5

p-adj. 0.1, |Log2FC| > 0.58

B

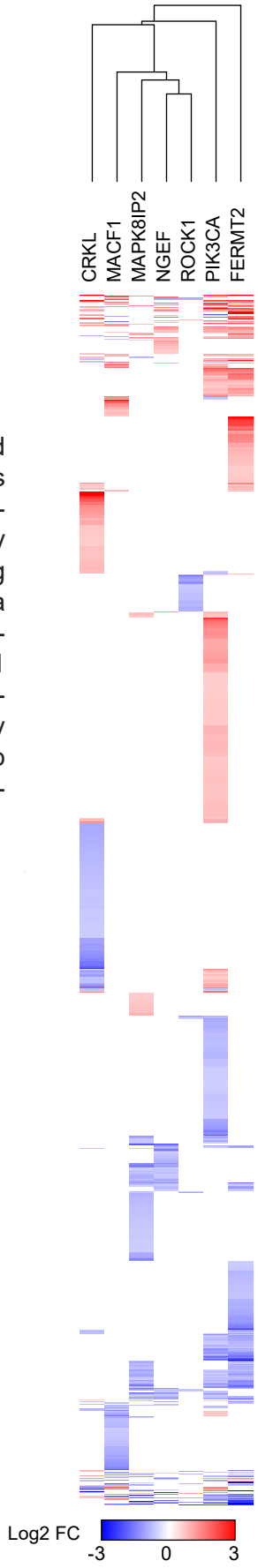

Figure S3. mRNA-Seq Analysis
(A) Cells were treated with the indicated siRNAs and after 48 hours total RNA was extracted and mRNA was sequenced using an Illumina workflow. The differentially expressed genes were obtained comparing expression to control-treated cells with a minimum of 3 biological replicas per condition. The p-adjusted value was set at 0.1 and the Log2FC at 0.58. **(B)** The differential expression analysis was hierarchically clustered and represented as a heat map using Morpheus (https://software.broadinstitute.org/morpheus).